# Spin-polarized neutron-rich matter at different orders of chiral effective field theory

F. Sammarruca,[1,*] R. Machleidt,[1] and N. Kaiser[2]

[1]*Department of Physics, University of Idaho, Moscow, Idaho 83844, USA*

[2]*Physik Department, Technische Universität München, D-85747 Garching, Germany*

(Received 20 May 2015; revised manuscript received 16 October 2015; published 30 November 2015)

Spin-polarized neutron matter is studied using chiral two- and three-body forces. We focus, in particular, on predictions of the energy per particle in ferromagnetic neutron matter at different orders of chiral effective field theory and for different choices of the resolution scale. We discuss the convergence pattern of the predictions and their cutoff dependence. We explore to what extent fully polarized neutron matter behaves (nearly) like a free Fermi gas. We also consider the more general case of partial polarization in neutron matter as well as the presence of a small proton fraction. In other words, in our calculations, we vary both spin and isospin asymmetries. Confirming the findings of other microscopic calculations performed with different approaches, we report no evidence for a transition to a polarized phase of neutron matter.

DOI: 10.1103/PhysRevC.92.054327 PACS number(s): 21.30.Fe, 21.65.Cd

## I. INTRODUCTION

The equation of state (EoS) of highly neutron-rich matter is a topic of current interest because of its many applications, ranging from the physics of rare isotopes to the properties of neutron stars. In spite of recent and fast-growing effort, the density dependence of the symmetry energy, which plays a chief role for the understanding of those systems, is not sufficiently constrained, and, at the same time, theoretical predictions show considerable model dependence.

Polarization properties of neutron and nuclear matter have been studied extensively with a variety of theoretical methods [1–25], often with contradictory conclusions. In the study in Ref. [24], for instance, the possibility of phase transitions into spin ordered states of symmetric nuclear matter was explored based on the Gogny interaction [5] and the Fermi liquid formalism. In that paper, the appearance of an antiferromagnetic state (with opposite spins for neutrons and protons) was predicted, whereas the transition to a ferromagnetic state was not indicated. This is in contrast to predictions based on Skyrme forces [25].

The properties of polarized neutron matter (NM) have gathered much attention lately, in conjunction with the issue of ferromagnetic instabilities together with the possibility of strong magnetic fields in the interior of rotating neutron stars. The presence of polarization would impact neutrino cross sections and luminosities, resulting in a very different scenario for neutron star cooling.

There are also other, equally important motivations to undertake studies of polarized matter. In Ref. [26], for instance, we focused on the spin degrees of freedom of symmetric nuclear matter (SNM), having in mind a terrestrial scenario as a possible "laboratory." We paid particular attention to the spin-dependent *symmetry potential*, namely the gradient between the single-nucleon potentials for upward and downward polarized nucleons in SNM. The interest around this quantity arises because of its natural interpretation as a spin-dependent nuclear optical potential, defined in perfect formal analogy to the Lane potential [27] for the isospin degree of freedom in isospin-asymmetric nuclear matter (IANM).

Whether one is interested in rapidly rotating pulsars or more conventional laboratory nuclear physics, it is important to consider both spin and isospin asymmetries. First, neutron star matter contains a non-negligible proton fraction. Concerning laboratory nuclear physics, one way to access information related to the spin dependence of the nuclear interaction in nuclear matter is the study of collective modes such as giant resonances. Because a spin unsaturated system is usually also isospin asymmetric, both degrees of freedom need to be taken into account. For those reasons, in previous calculations [28] we extended our predictions [26,29] to include matter with different concentrations of neutrons and protons, where each nucleon species can have definite spin polarization. Our framework was based on the Dirac-Brueckner-Hartree-Fock (DBHF) approach to nuclear matter together with a realistic meson-theoretic potential. Our findings did not show evidence of a phase transition to a ferromagnetic (FM) or antiferromagnetic (AFM) state. This conclusion appears to be shared by predictions of all microscopic models, such as those based on conventional Brueckner-Hartree-Fock theory [16]. On the other hand, calculations based on various parametrizations of Skyrme forces result in different conclusions. For instance, with the SLy4 and SLy5 forces and the Fermi liquid formalism a phase transition to the AFM state is predicted in asymmetric matter at a critical density equal to about 2–3 times normal density [24]. Qualitative disagreement is also encountered with other nonmicroscopic approaches such as relativistic Hartree-Fock models based on effective meson-nucleon Lagrangians. For instance, in Ref. [9] it was reported that the onset of a ferromagnetic transition in neutron matter, and its critical density, are crucially determined by the inclusion of isovector mesons and the nature of their couplings.

The brief review given above summarizes many useful and valid calculations. However, the problem common to all of them, including microscopic approaches, is that it is essentially impossible to estimate, in a statistically meaningful way, the uncertainties associated with a particular prediction, or to

*fsammarr@uidaho.edu

 

quantify the error related to the approximations applied in a particular model.

Effective field theories (EFTs) have shown the way out of this problem. Chiral effective field theory is a low-energy realization of QCD [30,31] which fits unresolved nuclear dynamics at short distances to the properties of two- and few-nucleon systems. Together with a power counting, chiral EFT provides a framework where two- and few-nucleon forces are generated on an equal footing in a systematic and controlled hierarchy.

Estimates of theoretical uncertainties [32] for calculations of the equation of state of nuclear and neutron matter have largely focused on varying the low-energy constants and resolution scale at which nuclear dynamics are probed [33–38]. In a recent work [39], we laid the foundations for order-by-order calculations of nuclear many-body systems by presenting consistent next-to-leading order (NLO) and next-to-next-to-leading order ($N^2LO$) chiral nuclear forces whose relevant short-range three-nucleon forces (3NFs) are fit to $A = 3$ binding energies and the lifetime of the triton [40]. We then assessed the accuracy with which infinite nuclear and neutron matter properties and the isospin asymmetry energy can be predicted from order-by-order calculations in chiral effective field theory. In this paper, we apply the same philosophy to study the equation of state of polarized neutron matter.

Based on the literature mentioned above, a phase transition to a polarized phase (at least up to normal densities) seems unlikely, although the validity of such a conclusion must be assessed in the context of EFT errors. Furthermore, polarized neutron matter is a very interesting system for several reasons. Because of the large neutron-neutron scattering length, NM displays behaviors similar to those of a unitary Fermi gas. In fact, up to nearly normal density, (unpolarized) neutron matter is found to display the behavior of an $S$-wave superfluid [41,42]. The possibility of simulating low-density NM with ultracold atoms near a Feshbach resonance [43] has also been discussed. When the system is totally polarized, it has been observed to behave like a weakly interacting Fermi gas [44]. Here, we wish to explore to what extent and up to what densities we are in agreement with such conclusions, and how this and other observations depend on the chiral order and the resolution scale.

In comparison with the calculations of Ref. [44] (where 3NFs and 4NFs up to $N^3LO$ were included), our present work contains the following novelties:

(1) We consider both cutoff dependence and truncation error for the purpose of uncertainty quantification of chiral EFT. Although incomplete in the 3NF at $N^3LO$, our calculations are a substantial step in that direction. We note, further, that the contribution from the 3NF at $N^3LO$ was found to be very small in neutron matter for the potentials in our perview [36]: about $-0.5$ MeV at normal density. Here, we consider neutron matter or highly neutron-rich matter.

(2) For the first time, we present results for both spin and isospin asymmetries within the framework of chiral forces. As discussed in Sec. III, these tools are necessary to assess, for instance, the sensitivity of the results (particularly, the potential onset of a phase transition) to the presence of a proton fraction.

This paper is organized as follows: In the next section, we present the formal aspects of the self-consistent calculation of the energy per particle, which are, in general, applicable to infinite matter with any degree of isospin and spin asymmetry. We also describe our approach to two- and three-body chiral forces. We provide expressions for the in-medium effective three-body force suitable for the most general case of different proton and neutron concentrations, where each species can be polarized to a different degree. To the best of our knowledge, this has not been reported before in the literature within the framework of chiral forces. Results for polarized and partially polarized NM, as well as for polarized neutron-rich matter in the presence of a small proton fraction, are discussed in Sec. III. Conclusions and future plans are summarized in Sec. IV.

## II. FORMALISM

### A. General aspects

In a spin-polarized and isospin asymmetric system with fixed total density $\rho$, the partial densities of each species are

$$\rho_n = \rho_{nu} + \rho_{nd}\,, \quad \rho_p = \rho_{pu} + \rho_{pd}\,, \quad \rho = \rho_n + \rho_p\,, \tag{1}$$

where $u$ and $d$ refer to up and down spin polarizations, respectively, of protons ($p$) or neutrons ($n$). The isospin and spin asymmetries $\alpha$, $\beta_n$, and $\beta_p$ are defined in a natural way:

$$\alpha = \frac{\rho_n - \rho_p}{\rho}, \quad \beta_n = \frac{\rho_{nu} - \rho_{nd}}{\rho_n}, \quad \beta_p = \frac{\rho_{pu} - \rho_{pd}}{\rho_p}. \tag{2}$$

The density of each individual component can be related to the total density by

$$\begin{aligned} \rho_{nu} &= (1+\beta_n)(1+\alpha)\frac{\rho}{4}, \quad \rho_{nd} = (1-\beta_n)(1+\alpha)\frac{\rho}{4}, \\ \rho_{pu} &= (1+\beta_p)(1-\alpha)\frac{\rho}{4}, \quad \rho_{pd} = (1-\beta_p)(1-\alpha)\frac{\rho}{4}, \end{aligned} \tag{3}$$

where each partial density is related to the corresponding Fermi momentum through $\rho_{\tau\sigma} = (k_F^{\tau\sigma})^3/(6\pi^2)$. The *average* Fermi momentum and the total density are related in the usual way as $\rho = (2k_F^3)/(3\pi^2)$.

The single-particle potential of a nucleon in a particular $\tau\sigma$ state, $U_{\tau\sigma}$, is the solution of a set of four coupled equations

$$U_{nu} = U_{nu,nu} + U_{nu,nd} + U_{nu,pu} + U_{nu,pd}\,, \tag{4}$$

$$U_{nd} = U_{nd,nu} + U_{nd,nd} + U_{nd,pu} + U_{nd,pd}\,, \tag{5}$$

$$U_{pu} = U_{pu,nu} + U_{pu,nd} + U_{pu,pu} + U_{pu,pd}\,, \tag{6}$$

$$U_{pd} = U_{pd,nu} + U_{pd,nd} + U_{pd,pu} + U_{pd,pd}, \tag{7}$$

to be solved self-consistently along with the effective interaction, the $G$ matrix. (The latter will be discussed in the next two subsections.) In the above equations, each $U_{\tau\sigma,\tau'\sigma'}$ term on the right-hand side contains the appropriate (spin and isospin dependent) part of the interaction, $G_{\tau\sigma,'\tau'\sigma'}$. More specifically,

$$U_{\tau\sigma,\tau'\sigma'}(\vec{k}) = \int_{|\vec{q}|<k_F^{\tau'\sigma'}} \frac{d^3q}{(2\pi)^3} \langle \tau\sigma,\tau'\sigma'|G(\vec{k},\vec{q})|\tau\sigma,\tau'\sigma'\rangle, \tag{8}$$

where the integration goes over the Fermi seas of protons and neutrons with spin up and spin down, and

$$\begin{aligned}&\langle \tau\sigma,\tau'\sigma'|G(\vec{k},\vec{q})|\sigma\tau,\sigma'\tau'\rangle\\ &= \sum_{L,L',S,J,M,M_L,T} \left|\left\langle \frac{1}{2}\sigma;\frac{1}{2}\sigma'\middle|S(\sigma+\sigma')\right\rangle\right|^2 \left|\left\langle \frac{1}{2}\tau;\frac{1}{2}\tau'\middle|T(\tau+\tau')\right\rangle\right|^2 \langle LM_L;S(\sigma+\sigma')|JM\rangle\langle L'M_L;S(\sigma+\sigma')|JM\rangle\\ &\quad\times i^{L'-L}Y^*_{L',M_L}(\hat{k}_{\rm rel})Y_{L,M_L}(\hat{k}_{\rm rel})\langle LSJ|G(k_{\rm rel},K_{c.m.})|L'SJ\rangle.\end{aligned} \tag{9}$$

The $G$ matrix that appears in the formulas above is constructed from the two-nucleon potential and the effective density-dependent 3NF, as explained later.

The need to separate the interaction by spin components brings along angular dependence, with the result that the single-particle potential depends also on the direction of the momentum, although such dependence was found to be weak [29]. The $G$-matrix equation is solved using partial wave decomposition and the matrix elements are then summed as in Eq. (9) to provide the new matrix elements in the representation needed for Eq. (8), namely with spin and isospin components explicitly projected out. Furthermore, the scattering equation is solved using relative and center-of-mass coordinates, $\vec{k}_{\rm rel}$ and $\vec{K}_{c.m.}$, since the former is a natural coordinate for the evaluation of the nuclear potential. Those are then easily related to the momenta of the two particles, $\vec{k}$ and $\vec{q}$, in order to perform the integration indicated in Eq. (8). Notice that solving the $G$-matrix equation requires knowledge of the single-particle potential, which in turn requires knowledge of the effective interaction. Hence, Eqs. (4)–(7) together with the $G$-matrix equation constitute a rather lengthy self-consistency problem, the solution of which yields the single-nucleon potentials in each $\tau\sigma$ channel.

The kernel of the $G$-matrix equation contains the Pauli operator for scattering of two particles with two different Fermi momenta, $k_F^{\tau\sigma}$ and $k_F^{\tau'\sigma'}$, which is defined in analogy with the one for isospin-asymmetric matter [45],

$$Q_{\tau\sigma,\tau'\sigma'}(k,q,k_F^{\tau\sigma},k_F^{\tau'\sigma'}) = \begin{cases} 1 & \text{if} \quad k > k_F^{\tau\sigma} \text{ and } q > k_F^{\tau'\sigma'} \\ 0 & \text{otherwise.} \end{cases} \tag{10}$$

The Pauli operator is expressed in terms of $\vec{k}_{\rm rel}$ and $\vec{K}_{c.m.}$ and angle averaged in the usual way. We then proceed with the calculation of the energy per nucleon in the particle-particle ladder approximation, namely the leading-order contribution in the hole-line expansion. (See Ref. [39], and references therein for a discussion of the uncertainty associated with this approximation.)

Once a self-consistent solution for Eqs. (4)–(7) has been obtained, the average potential energy for a given $\tau\sigma$ component can be calculated. A final average over all $\tau\sigma$ components provides, along with the kinetic energy $K_{\tau\sigma}$, the average energy per particle $E/A$ in spin-polarized isospin-asymmetric nuclear matter. Specifically,

$$\frac{E}{A} = \sum_{\sigma=u,d}\sum_{\tau=n,p}\frac{1}{\rho}\int_{|\vec{k}|<k_F^{\tau\sigma}} \frac{d^3k}{(2\pi)^3}\Big(K_{\tau\sigma}(k) + \frac{1}{2}U_{\tau\sigma}(k)\Big), \tag{11}$$

where $E/A$ is a function of $\rho$, $\alpha$, $\beta_n$, and $\beta_p$, with $\alpha = 1$ in the present case. All calculations are conducted including values of the total angular momentum $J$ from 0 to 15.

### B. Chiral two-body potentials

In this section we discuss in some detail the features of the nucleon-nucleon ($NN$) potentials we use for these calculations.

All low-momentum interactions are limited in calculations of the EoS to densities where the characteristic momentum scale (on the order of the Fermi momentum) is below the scale set by the momentum-space cutoff $\Lambda$ in the $NN$ potential regulating function, which for chiral $NN$ forces typically has the form

$$f(p',p) = \exp[-(p'/\Lambda)^{2n} - (p/\Lambda)^{2n}], \tag{12}$$

where $\Lambda \lesssim 500$ MeV is associated with the onset of favorable perturbative properties [37,38].

Although designed to reproduce similar $NN$ scattering phase shifts, $NN$ potentials with different regulator functions will yield different predictions in the nuclear many-body problem due to their different off-shell behavior. On the other hand, appropriate readjustment of the low-energy constants that appear in the nuclear many-body forces is expected to reduce the dependence on the regulator function [37].

In the present investigation we consider $NN$ potentials at order $(q/\Lambda_\chi)^2$, $(q/\Lambda_\chi)^3$, and $(q/\Lambda_\chi)^4$ in the chiral power counting, where $q$ denotes the small scale set by external nucleon momenta or the pion mass and $\Lambda_\chi$ is the chiral symmetry breaking scale. Chiral $NN$ potentials at NLO and N$^2$LO, corresponding to $(q/\Lambda_\chi)^2$ and $(q/\Lambda_\chi)^3$, have been constructed previously in Ref. [46] for cutoffs ranging from $\Lambda = 450$ to about 800 MeV. With varying chiral order and cutoff scale, the low-energy constants in the two-nucleon sector are refitted to elastic $NN$ scattering phase shifts and properties of the deuteron. The low-energy constants $c_{1,3,4}$ associated with the $\pi\pi NN$ contact couplings of the $\mathcal{L}^{(2)}_{\pi N}$ chiral Lagrangian are given in Table I. We note that the $c_i$ can be extracted from $\pi N$ or $NN$ scattering data. The potentials we use here [47,48] follow the second path. At N$^2$LO, taking

TABLE I. Values of $n$ and low-energy constants of the dimension-two $\pi N$ Lagrangian, $c_{1,3,4}$, at each order and for each type of cutoff in the regulator function given in Eq. (12). None of the $c_i$'s appears at NLO. The low-energy constants are given in units of GeV$^{-1}$.

| NLO | $\Lambda$ (MeV) | $n$ | $c_1$ | $c_3$ | $c_4$ |
|---|---|---|---|---|---|
| | 450 | 2 | | | |
| | 500 | 2 | | | |
| | 600 | 2 | | | |
| N$^2$LO | $\Lambda$ (MeV) | $n$ | $c_1$ | $c_3$ | $c_4$ |
| | 450 | 3 | −0.81 | −3.40 | 3.40 |
| | 500 | 3 | −0.81 | −3.40 | 3.40 |
| | 600 | 3 | −0.81 | −3.40 | 3.40 |
| N$^3$LO | $\Lambda$ (MeV) | $n$ | $c_1$ | $c_3$ | $c_4$ |
| | 450 | 3 | −0.81 | −3.40 | 3.40 |
| | 500 | 2 | −0.81 | −3.20 | 5.40 |
| | 600 | 2 | −0.81 | −3.20 | 5.40 |

the range determined in analyses of elastic $\pi N$ scattering as a starting point, values were chosen to best reproduce $NN$ data at that order. At N$^3$LO, high precision required a stronger adjustment of $c_4$ depending on the regulator function and cutoff. The fitting procedure is discussed in Ref. [48], where it is noted that the larger value for $c_4$ has, overall, a very small impact but lowers the $^3F_2$ phase shift for a better agreement with the phase shift analysis.

In Ref. [46], it was found that the two-body scattering phase shifts can be described well at NLO up to a laboratory energy of about 100 MeV, while the N$^2$LO potential fits the data up to 200 MeV. Interestingly, in the latter case the $\chi^2$/datum was found to be essentially cutoff independent for variations of $\Lambda$ between 450 and approximately 800 MeV. Finally, we also use $NN$ potentials constructed at next-to-next-to-next-to-leading order (N$^3$LO) [47,48], with low-energy constants $c_{1,3,4}$ as displayed in Table I.

Although N$^2$LO calculations can achieve sufficient accuracy in selected partial wave channels up to $E_{\rm lab} = 200$ MeV, only the N$^3$LO interactions achieve the level of high-precision potentials, characterized by a $\chi^2$/datum $\simeq 1$.

At the two-body level, each time the chiral order is increased, the $NN$ contact terms and/or the two-pion-exchange contributions proportional to the low-energy constants $c_{1,3,4}$ are refitted. We recall that at N$^2$LO no new $NN$ contact terms are generated, and therefore improved cutoff independence in the $NN$ phase shifts [39] is due to changes in the two-pion-exchange contributions. At N$^2$LO, subleading $\pi\pi NN$ vertices enter into the chiral $NN$ potential. These terms encode the important physics of correlated two-pion exchange and the excitation of intermediate $\Delta(1232)$ isobar states. Therefore, at this order it is possible to obtain a realistic description of the $NN$ interaction at intermediate range, traditionally generated through the exchange of a fictitious $\sigma$ meson of medium mass. At N$^3$LO in the chiral power counting, 15 additional $NN$ contact terms (bringing the total number to 24 at N$^3$LO) result in a much improved description of $NN$ scattering phase shifts.

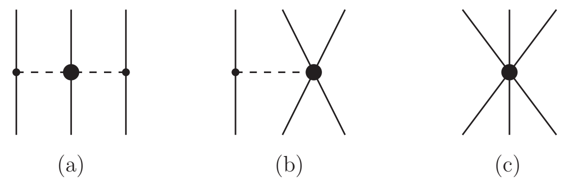


FIG. 1. Diagrams for the chiral three-nucleon interaction at N$^2$LO. In neutron matter, only diagram (a) contributes.

### C. The three-nucleon force

The leading three-nucleon force makes its appearance at third order in the chiral power counting and contains three contributions: the long-range two-pion-exchange part with $\pi\pi NN$ vertex proportional to the low-energy constants $c_1,c_3,c_4$, the medium-range one-pion exchange diagram proportional to the low-energy constant $c_D$, and finally the short-range contact term proportional to $c_E$. The corresponding diagrams are shown in Fig. 1, labeled as (a), (b), and (c), respectively. Diagrams (b) and (c) vanish in neutron matter, while all three terms contribute in symmetric nuclear matter [49,50].

Although efforts are in progress to incorporate potentially important N$^3$LO 3NF contributions [51–53] both in neutron and nuclear matter equations of state and the fitting of the relevant low-energy constants, the "N$^3$LO" study reported in this paper is limited to the inclusion of the N$^2$LO three-body force together with the N$^3$LO two-body force, an approximation that is commonly used in the literature. The associated uncertainties for neutron matter have been investigated in Ref. [39].

To facilitate the inclusion of 3NFs in the particle-particle ladder calculation, we employ the density-dependent $NN$ interaction derived in Refs. [49,54] from the N$^2$LO chiral three-body force. This effective interaction is obtained by summing one particle line over the occupied states in the Fermi sea. Neglecting small contributions [50] from terms depending on the center-of-mass momentum, the resulting $NN$ interaction can be expressed in analytical form with operator structures identical to those of free-space $NN$ interactions, and which are therefore included on the same footing as two-body forces. The small uncertainty associated with the use of these effective density-dependent 3NFs was discussed in Ref. [39].

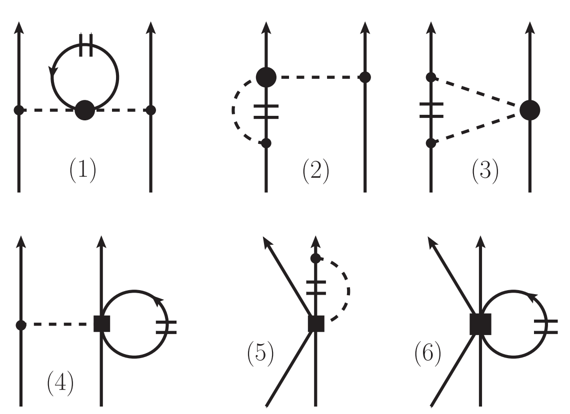


FIG. 2. Diagrams for the in-medium $NN$ interactions corresponding to $V_{NN}^{{\rm med},i}$ $(i = 1,\ldots,6)$ given in the text.

For the case of polarized isospin-asymmetric matter, the expressions from Ref. [49] are to be extended to include four different Fermi momenta, namely those of upward(downward) polarized neutrons(protons), as described below.

Using the notation established above to indicate the Fermi momenta of spin-up and spin-down neutrons or protons, the neutron and proton densities are given by $\rho_n = [(k_F^{nu})^3 + (k_F^{nd})^3]/6\pi^2$ and $\rho_p = [(k_F^{pu})^3 + (k_F^{pd})^3]/6\pi^2$. Concerning kinematics, we consider elastic scattering process $N_1(\vec{p}\,) + N_2(-\vec{p}\,) \to N_1(\vec{p} + \vec{q}\,) + N_2(-\vec{p} - \vec{q}\,)$ in the center-of-mass frame.

Following the notation of Ref. [49], we can distinguish between six effective density-dependent $NN$ interactions, represented by the diagrams (1) to (6) in Fig. 2. They are the following:

The Pauli blocked pion self-energy [diagram (1)] is

$$V_{NN}^{\mathrm{med},1} = \frac{g_A^2}{2f_\pi^4}\,\vec{\tau}_1\cdot\vec{\tau}_2\,\frac{\vec{\sigma}_1\cdot\vec{q}\,\vec{\sigma}_2\cdot\vec{q}}{\left(m_\pi^2+q^2\right)^2}\left(2c_1m_\pi^2 + c_3q^2\right)(\rho_p+\rho_n). \tag{13}$$

The Pauli blocked vertex correction [diagram (2)] is

$$\begin{aligned}
V_{NN}^{\mathrm{med},2} = {}& \frac{g_A^2}{16\pi^2 f_\pi^4}\vec{\tau}_1\cdot\vec{\tau}_2\,\frac{\vec{\sigma}_1\cdot\vec{q}\,\vec{\sigma}_2\cdot\vec{q}}{m_\pi^2+q^2}\{-4c_1m_\pi^2[\Gamma_0^+(p)+\Gamma_1^+(p)] - (c_3+c_4)\\
&\times[q^2(\Gamma_0^+(p)+2\Gamma_1^+(p)+\Gamma_3^+(p)) + 4\Gamma_2^+(p)] + 4c_4\big[2\pi^2(\rho_p+\rho_n) - m_\pi^2\Gamma_0^+(p)\big]\big\}\\
&+\frac{g_A^2}{32\pi^2 f_\pi^4}\big(\tau_1^3+\tau_2^3\big)\frac{\vec{\sigma}_1\cdot\vec{q}\,\vec{\sigma}_2\cdot\vec{q}}{m_\pi^2+q^2}\{-4c_1m_\pi^2[\Gamma_0^-(p)+\Gamma_1^-(p)] + (c_4-c_3)\\
&\times[q^2(\Gamma_0^-(p)+2\Gamma_1^-(p)+\Gamma_3^-(p)) + 4\Gamma_2^-(p)] + 4c_4\big[2\pi^2(\rho_n-\rho_p) + m_\pi^2\Gamma_0^-(p)\big]\big\}\\
&+\frac{g_A^2}{16\pi^2 f_\pi^4}\big(\tau_1^3-\tau_2^3\big)\,i(\vec{\sigma}_1-\vec{\sigma}_2)\cdot(\vec{p}\times\vec{q}\,)\frac{1}{m_\pi^2+4p^2-q^2}\\
&\times\big\{4c_1m_\pi^2[\Gamma_0^-(p)+\Gamma_1^-(p)] + c_3(4p^2-q^2)[\Gamma_0^-(p)+2\Gamma_1^-(p)+\Gamma_3^-(p)]\big\},
\end{aligned} \tag{14}$$

The last contribution, proportional to $(\tau_1^3-\tau_2^3)$, leads to spin-singlet and spin-triplet mixing in the medium. It has been Fierz transformed to bring it into the form of the antisymmetric spin-orbit operator $i(\vec{\sigma}_1-\vec{\sigma}_2)\cdot(\vec{p}\times\vec{q}\,)$. Terms which break rotational invariance in momentum-space due to the spin-polarization of the nuclear medium in the $z$-direction have been discarded.

Next, we give the expression for the Pauli blocked two-pion exchange [diagram (3)]:

$$\begin{aligned}
V_{NN}^{\mathrm{med},3} = {}& \frac{g_A^2}{32\pi^2 f_\pi^4}\{-12c_1m_\pi^2\big[2\Gamma_0^+(p) - \big(2m_\pi^2+q^2\big)G_0^+(p,q)\big]\\
&-3c_3\big[8\pi^2(\rho_p+\rho_n) - 4\big(2m_\pi^2+q^2\big)\Gamma_0^+(p) - 2q^2\Gamma_1^+(p) + \big(2m_\pi^2+q^2\big)^2G_0^+(p,q)\big]\\
&+4c_4\,\vec{\tau}_1\cdot\vec{\tau}_2\,(\vec{\sigma}_1\cdot\vec{\sigma}_2\,q^2 - \vec{\sigma}_1\cdot\vec{q}\,\vec{\sigma}_2\cdot\vec{q}\,)G_2^+(p,q)\\
&-(3c_3+c_4\vec{\tau}_1\cdot\vec{\tau}_2)\,i(\vec{\sigma}_1+\vec{\sigma}_2)\cdot(\vec{q}\times\vec{p}\,)\big[2\Gamma_0^+(p) + 2\Gamma_1^+(p) - \big(2m_\pi^2+q^2\big)\\
&\times(G_0^+(p,q)+2G_1^+(p,q))\big] - 12c_1m_\pi^2\,i(\vec{\sigma}_1+\vec{\sigma}_2)\cdot(\vec{q}\times\vec{p}\,)[G_0^+(p,q)+2G_1^+(p,q)]\\
&+4c_4\,\vec{\tau}_1\cdot\vec{\tau}_2\,\vec{\sigma}_1\cdot(\vec{q}\times\vec{p}\,)\,\vec{\sigma}_2\cdot(\vec{q}\times\vec{p}\,)[G_0^+(p,q)+4G_1^+(p,q)+4G_3^+(p,q)]\big\}\\
&+\frac{g_A^2}{64\pi^2 f_\pi^4}\big(\tau_1^3+\tau_2^3\big)\{4c_1m_\pi^2\big[2\Gamma_0^-(p) - \big(2m_\pi^2+q^2\big)G_0^-(p,q)\big]\\
&+c_3\big[8\pi^2(\rho_p-\rho_n) - 4\big(2m_\pi^2+q^2\big)\Gamma_0^-(p) - 2q^2\Gamma_1^-(p) + \big(2m_\pi^2+q^2\big)^2G_0^-(p,q)\big]\\
&-4c_4\,(\vec{\sigma}_1\cdot\vec{\sigma}_2\,q^2 - \vec{\sigma}_1\cdot\vec{q}\,\vec{\sigma}_2\cdot\vec{q}\,)G_2^-(p,q)\\
&+(c_3+c_4)\,i(\vec{\sigma}_1+\vec{\sigma}_2)\cdot(\vec{q}\times\vec{p}\,)\big[2\Gamma_0^-(p) + 2\Gamma_1^-(p) - \big(2m_\pi^2+q^2\big)\\
&\times(G_0^-(p,q)+2G_1^-(p,q))\big] + 4c_1m_\pi^2\,i(\vec{\sigma}_1+\vec{\sigma}_2)\cdot(\vec{q}\times\vec{p}\,)[G_0^-(p,q)+2G_1^-(p,q)]\\
&-4c_4\,\vec{\sigma}_1\cdot(\vec{q}\times\vec{p}\,)\,\vec{\sigma}_2\cdot(\vec{q}\times\vec{p}\,)[G_0^-(p,q)+4G_1^-(p,q)+4G_3^-(p,q)]\big\}.
\end{aligned} \tag{15}$$

The loop functions $\Gamma_j^{\pm}(p)$ and $G_j^{\pm}(p,q)$ with a superscript + or − are given by

$$\Gamma_j^{\pm}(p) = \tfrac{1}{2}[\Gamma_j(p,k_{pu}) + \Gamma_j(p,k_{pd})] \pm \tfrac{1}{2}[\Gamma_j(p,k_{nu}) + \Gamma_j(p,k_{nd})], \tag{16}$$

$$G_j^{\pm}(p,q) = \tfrac{1}{2}[G_j(p,q,k_{pu}) + G_j(p,q,k_{pd})] \pm \tfrac{1}{2}[G_j(p,q,k_{nu}) + G_j(p,q,k_{nd})], \tag{17}$$

where $\Gamma_j(p,k_f)$ and $G(p,q,k_f)$ are defined in Eqs. (13)–(16) and Eqs. (18)–(22) of Ref. [49].

Now we present the contributions from the $1\pi$-exchange 3NF proportional to the low-energy constant $c_D$. The vertex correction to $1\pi$ exchange linear in proton and neutron densities is [diagram (4)]

$$V_{NN}^{\mathrm{med},4} = \frac{g_A c_D}{16 f_\pi^4 \Lambda_\chi}\left[-2\vec{\tau}_1\cdot\vec{\tau}_2(\rho_p+\rho_n) + \left(\tau_1^3+\tau_2^3\right)(\rho_p-\rho_n)\right]\frac{\vec{\sigma}_1\cdot\vec{q}\,\vec{\sigma}_2\cdot\vec{q}}{m_\pi^2+q^2}\,. \tag{18}$$

Pauli blocking in the vertex correction [diagram (5)] contributes in the form

$$\begin{aligned}V_{NN}^{\mathrm{med},5} = {}& \frac{g_A c_D}{32\pi^2 f_\pi^4 \Lambda_\chi}\Bigg\{\vec{\tau}_1\cdot\vec{\tau}_2\Bigg[2\vec{\sigma}_1\cdot\vec{\sigma}_2\,\Gamma_2^+(p) + \Bigg(\vec{\sigma}_1\cdot\vec{\sigma}_2\left(2p^2-\frac{q^2}{2}\right) + \vec{\sigma}_1\cdot\vec{q}\,\vec{\sigma}_2\cdot\vec{q}\\
&\times\left(1-\frac{2p^2}{q^2}\right) - \frac{2}{q^2}\,\vec{\sigma}_1\cdot(\vec{q}\times\vec{p}\,)\vec{\sigma}_2\cdot(\vec{q}\times\vec{p}\,)\Bigg)[\Gamma_0^+(p)+2\Gamma_1^+(p)+\Gamma_3^+(p)]\Bigg] + 12\pi^2(\rho_p+\rho_n) - 6m_\pi^2\Gamma_0^+(p)\Bigg\}\\
&+ \frac{g_A c_D}{64\pi^2 f_\pi^4 \Lambda_\chi}\left(\tau_1^3+\tau_2^3\right)\Bigg\{2\vec{\sigma}_1\cdot\vec{\sigma}_2\,\Gamma_2^-(p) + \Bigg[\vec{\sigma}_1\cdot\vec{\sigma}_2\left(2p^2-\frac{q^2}{2}\right) + \vec{\sigma}_1\cdot\vec{q}\,\vec{\sigma}_2\cdot\vec{q}\\
&\times\left(1-\frac{2p^2}{q^2}\right) - \frac{2}{q^2}\,\vec{\sigma}_1\cdot(\vec{q}\times\vec{p}\,)\vec{\sigma}_2\cdot(\vec{q}\times\vec{p}\,)\Bigg][\Gamma_0^-(p)+2\Gamma_1^-(p)+\Gamma_3^-(p)] + 4\pi^2(\rho_n-\rho_p) + 2m_\pi^2\Gamma_0^-(p)\Bigg\}.\end{aligned} \tag{19}$$

The contribution from the contact 3NF proportional to the low-energy constant $c_E$ is [diagram (6)]

$$V_{NN}^{\mathrm{med},6} = \frac{3c_E}{4 f_\pi^4 \Lambda_\chi}\left[-2(\rho_p+\rho_n) + (\rho_p-\rho_n)\left(\tau_1^3+\tau_2^3\right)\right]. \tag{20}$$

Partial wave matrix elements with $J \geqslant 1$ of the antisymmetric spin-orbit term, which occur in Eq. (14), mix spin-singlet and spin-triplet states, and these can be calculated for on-shell kinematics in the center-of-mass frame as

$$\begin{aligned}\langle J0J|i(\vec{\sigma}_1-\vec{\sigma}_2)\cdot(\vec{p}\times\vec{q}\,)F(q^2)|J1J\rangle &= \langle J1J|i(\vec{\sigma}_1-\vec{\sigma}_2)\cdot(\vec{p}\times\vec{q}\,)F(p^2,q^2)|J0J\rangle\\
&= \frac{\sqrt{J(J+1)}}{2J+1}\int_{-1}^{1} dz\, p^2 F(p^2,2p^2(1-z))[P_{J-1}(z)-P_{J+1}(z)].\end{aligned} \tag{21}$$

However, because of the small size of this contribution, particularly for small proton fractions, we neglect this term in the present calculations.

### III. RESULTS AND DISCUSSION

We show in Fig. 3 the energy per particle in fully polarized neutron matter as a function of density. The yellow and red bands represent the predictions of complete calculations at second and third order, respectively, of chiral effective field theory, while the blue band shows the predictions obtained with the exploratory N$^3$LO calculation as described above. For each band, the width is obtained by changing the cutoff between 450 MeV and 600 MeV.

At N$^2$LO and N$^3$LO, cutoff dependence is generally moderate up to saturation density. At NLO, the cutoff dependence is practically negligible throughout. In unpolarized neutron matter, on the other hand, the largest cutoff dependence was seen at NLO [39]. This suggests that, in unpolarized NM, the larger cutoff sensitivity at NLO is mostly due to singlet states, particularly $^1S_0$, which are absent from the polarized system. At the same time, 3NFs do not appear at NLO, implying that most of the cutoff dependence in polarized NM at N$^2$LO and N$^3$LO is caused by the 3NF contributions.

Clearly, the variations associated with changing the cutoff are not a good indicator of the uncertainty at a given order of chiral effective field theory, as the results from one order to the other do not overlap. Furthermore, the predictions do not show a good convergence pattern, although some indication of slow convergence can be seen when moving from N$^2$LO to our N$^3$LO calculation.

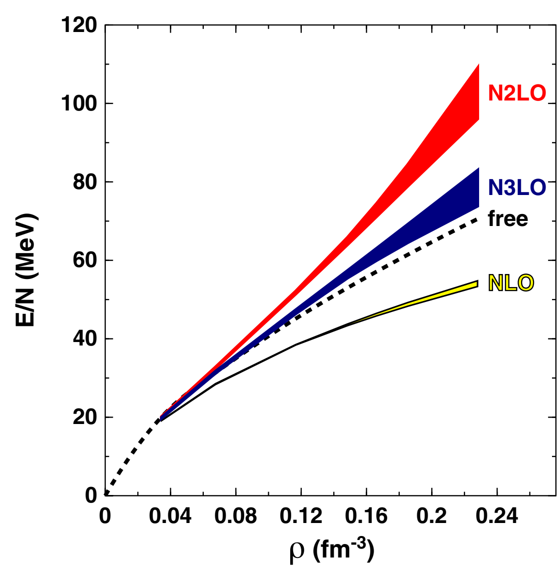


FIG. 3. (Color online) Energy per neutron in fully polarized neutron matter as a function of density. The yellow and red bands represent the uncertainties due to cutoff variations obtained in the complete calculations at NLO and N$^2$LO, respectively. The blue band is the result of the same cutoff variations applied to our exploratory N$^3$LO calculation; see text for details. The dotted curve shows the energy of the free Fermi gas.

TABLE II. Ratio of the energy per particle of a free Fermi gas to the energy per particle of polarized neutron matter around saturation density at N$^3$LO (as described in the text) and for different values of the cutoff.

| Density (fm$^{-3}$) | $\Lambda$ (MeV) | $E_{FFG}/E$ |
|---|---|---|
| 0.15 | 450 | 0.95 |
| | 500 | 0.92 |
| | 600 | 0.95 |
| 0.17 | 450 | 0.95 |
| | 500 | 0.91 |
| | 600 | 0.93 |

As can be concluded from Table II, the predictions from the N$^3$LO calculation are close to the free Fermi gas energy, at least up to saturation densities. Our results with the N$^3$LO ($\Lambda =$ 500 MeV) potential are in good agreement with those from Ref. [44] using the same potential as well as three- and four-nucleon forces at N$^3$LO. With regard to the similarity with the free Fermi gas, it is interesting to include some additional considerations. As mentioned in the Introduction, many-fermion systems with large scattering lengths offer the opportunity to model low-density neutron matter. In the unitary limit (that is, when the system can support a bound state at zero energy), the scattering length approaches infinity. The system then becomes scale independent and the ground-state energy is determined by a single universal parameter, known as the Bertsch parameter, $\xi$. The latter is defined as the ratio of the energy per particle of the unitary gas to that of the free Fermi gas. In Ref. [55], using a contact interaction proportional to the diverging scattering length, $a_{nn} \to \infty$, and resumming the combined particle-particle and hole-hole ladder diagrams to all orders, it was found that $\xi$ increases from approximately 0.5 to 1.0 as the spin asymmetry of neutron matter, $\beta_n$, is increased from 0 (unpolarized) to 1 (fully polarized).

In Fig. 4, for our N$^3$LO calculation, we compare predictions (along with their cutoff variations) of the energy per neutron in unpolarized NM (green band), partially polarized NM (pink band), and fully polarized NM (blue band). For the partially polarized case, the value of $\beta_n$ [see Eq. (2)] is equal to 0.5, corresponding to 75% of the neutrons being polarized in one direction and 25% in the opposite direction; see Eqs. (3) and (4). Clearly, a lesser degree of spin asymmetry (as compared to the ferromagnetic case) yields considerably more attraction. (At $\beta_n = 1$ interactions all together become very small.) There is definitely no sign of a phase transition, particularly to a ferromagnetic state, nor an indication that such transition may occur at higher densities. This is consistent with what we observed earlier [28] with meson-theoretic interactions.

As a baseline comparison, we also include, for the unpolarized case, predictions based on a different approach, shown by the black dotted line in Fig. 4. These are taken from Ref. [56] and are based on the Argonne $v_{18}$ two-nucleon interaction plus the Urbana IX three-body force, using variational methods. The predictions are overall in reasonable agreement with our green band, although those from Ref. [56] show more repulsion as compared to the softer chiral interactions.

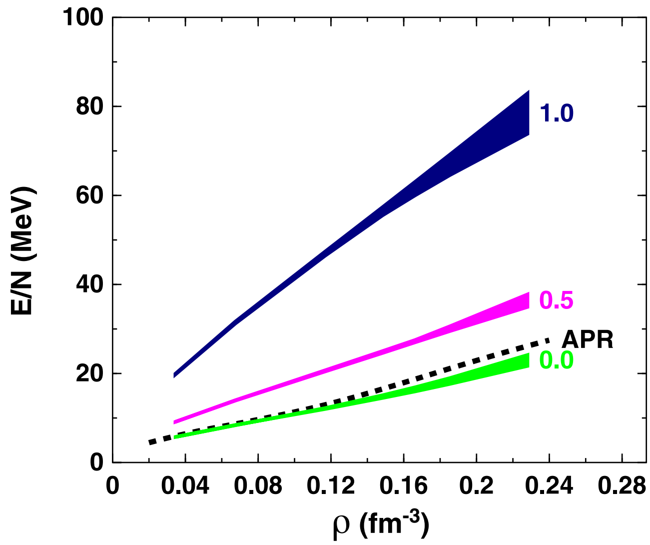


FIG. 4. (Color online) Energy per neutron in pure neutron matter as a function of density at N$^3$LO. From lowest to highest curve: unpolarized NM; partially polarized NM, with $\beta_n = 0.5$; fully polarized NM ($\beta_n = 1$). The width of each band shows the uncertainty from varying the cutoff between 450 and 600 MeV. The black dotted line shows the predictions for the equation of state of unpolarized neutron matter from Ref. [56].

Most typically, models which do predict spin instability of neutron matter find the phase transition to occur at densities a few times normal density. Such high densities are outside

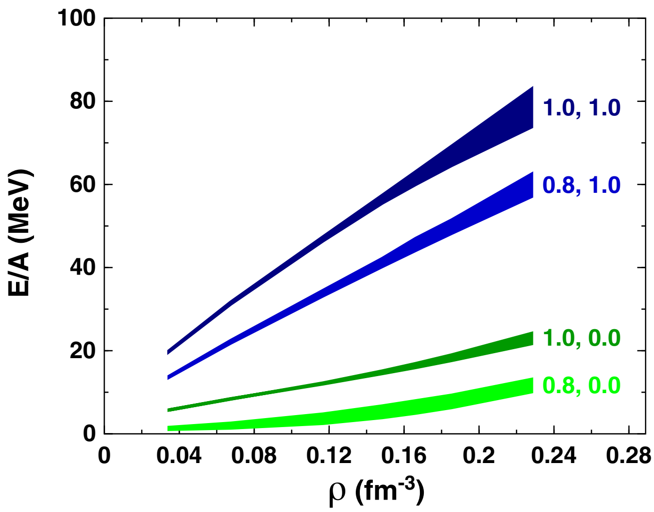


FIG. 5. (Color online) Energy per nucleon in neutron-rich matter as a function of density at N$^3$LO and different conditions of isospin and spin polarization. The brighter blue band labeled as "0.8, 1.0" displays the results for neutron-rich matter with a proton fraction equal to 10% ($\alpha = 0.8$) and fully polarized neutron ($\beta_n = 1.0$). The brighter green band labeled as "0.8, 0.0" refers to neutron-rich matter with the same proton fraction and no polarization ($\beta_n = 0.0$). The protons are unpolarized. For comparison, we also include the bands (darker blue and darker green) already shown in the previous figure, which refer to pure neutron matter ($\alpha = 1$) with fully polarized ($\beta_n =$ 1) or unpolarized ($\beta_n = 0$) neutrons. The bands are obtained varying the cutoff between 450 and 600 MeV.

the domain of chiral effective field theory. With some effective forces, though, it was found [17] that a small fraction of protons can significantly reduce the onset of the threshold density for a phase transition to a spin-polarized state of neutron-rich matter. We explored this scenario by adding a small fraction of protons to fully polarized or unpolarized neutrons. From Eqs. (1)–(3), a proton fraction of 10% is obtained with $\alpha = 0.8$. The results are displayed in Fig. 5, where a crossing of the bands labeled with "0.8, 1.0" and "0.8, 0.0", respectively, would indicate a phase transition. Thus we conclude that such transition is not predicted with chiral forces. By extrapolation, a transition to a polarized state would also appear very unlikely at higher densities.

## IV. CONCLUSIONS AND OUTLOOK

We have calculated the equation of state of (fully and partially) polarized neutron-rich matter. We performed complete calculations at second and third order of chiral effective field theory and calculations employing the N$^3$LO 2NF plus the leading 3NF. Results with both spin and isospin asymmetries are presented for the first time with chiral forces.

In all calculations, the cutoff dependence is moderate and definitely underestimates the uncertainty of each order. Concerning the latter, we do not see a satisfactory convergence pattern. The missing 3NFs are most likely not the main cause of uncertainty at N$^3$LO, since Ref. [44] has demonstrated that large cancelations take place between the $2\pi$-exchange 3NF and the $\pi$-ring 3NF at N$^3$LO, while other 3NF contributions are very small (about 0.1–0.2 MeV). Clearly a calculation at N$^4$LO is absolutely necessary to get a realistic indication of the EFT error at N$^3$LO. Such effort is in progress. If such calculation displays a reasonable convergence pattern, it will be strong evidence that polarized neutron matter, indeed, behaves nearly like a free Fermi gas, at least up to normal densities.

In our N$^3$LO calculation, the energies of the unpolarized system at normal density are close to 16 MeV for all cutoffs, whereas those in the polarized case are approximately 60 MeV. Thus, even in the presence of the large uncertainties discussed above, a phase transition to a ferromagnetic state can be excluded. This conclusion remaind valid in the presence of a small proton fraction.

## ACKNOWLEDGMENTS

This work was supported in part by the U.S. Department of Energy Office of Science, Office of Basic Energy Sciences, under Grant No. DE-FG02-03ER41270 (F.S. and R.M.), and by DFG and NSFC (CRC110) (N.K.).

[1] J. M. Pearson and G. Saunier, Phys. Rev. Lett. **24**, 325 (1970).
[2] V. R. Pandharipande, V. K. Garde, and J. K. Srivastava, Phys. Lett. B **38**, 485 (1972).
[3] S. O. Bäckmann and C. G. Källman, Phys. Lett. B **43**, 263 (1973).
[4] P. Haensel, Phys. Rev. C **11**, 1822 (1975).
[5] J. Decharge and D. Gogny, Phys. Rev. C **21**, 1568 (1980).
[6] J. Dabrowski, Can. J. Phys. **62**, 400 (1984).
[7] M. Kutshera and W. Wojcik, Phys. Lett. B **223**, 11 (1989).
[8] A. Vidaurre, J. Navarro, and J. Bernabéu, Astron. Astrophys. **135**, 361 (1984).
[9] S. Marcos, R. Niembro, M. L. Quelle, and J. Navarro, Phys. Lett. B **271**, 277 (1991).
[10] M. Kutschera and W. Wójcik, Phys. Lett. B **325**, 271 (1994).
[11] P. Bernardos, S. Marcos, R. Niembro, and M. L. Quelle, Phys. Lett. B **356**, 175 (1995).
[12] V. S. Uma Maheswari, D. N. Basu, J. N. De, and S. K. Samaddar, Nucl. Phys. A **615**, 516 (1997).
[13] S. Fantoni, A. Sarsa, and K. E. Schmidt, Phys. Lett. **87**, 181101 (2001).
[14] T. Frick, H. Müther, and A. Sedrakian, Phys. Rev. C **65**, 061303 (2002).
[15] I. Vidaña, A. Polls, and A. Ramos, Phys. Rev. C **65**, 035804 (2002).
[16] I. Vidaña and Ignazio Bombaci, Phys. Rev. C **66**, 045801 (2002).
[17] A. A. Isayev and J. Yang, Phys. Rev. C **69**, 025801 (2004).
[18] F. L. Braghin, Phys. Rev. C **71**, 064303 (2005).
[19] N. Kaiser, Phys. Rev. C **70**, 054001 (2004).
[20] A. Rios, A. Polls, and I. Vidaña, Phys. Rev. C **71**, 055802 (2005).
[21] I. Bombaci, A. Polls, A. Ramos, A. Rios, and I. Vidaña, Phys. Lett. B **632**, 638 (2006).
[22] W. Zuo, U. Lombardo, and C. W. Shen, in *Quark-Gluon Plasma and Heavy Ion Collisions*, edited by W. M. Alberico *et al.* (World Scientific, Singapore, 2002), p. 192.
[23] W. Zuo, Caiwan Shen, and U. Lombardo, Phys. Rev. C **67**, 037301 (2003).
[24] A. A. Isayev and J. Yang, Phys. Rev. C **70**, 064310 (2004).
[25] A. A. Isayev, JETP Lett. **77**, 251 (2003).
[26] F. Sammarruca, Phys. Rev. C **82**, 027307 (2010).
[27] A. M. Lane, Nucl. Phys. **35**, 676 (1962).
[28] F. Sammarruca, Phys. Rev. C **83**, 064304 (2011).
[29] F. Sammarruca and P. G. Krastev, Phys. Rev. C **75**, 034315 (2007).
[30] S. Weinberg, Phys. Rev. **166**, 1568 (1968).
[31] S. Weinberg, Physica A **96**, 327 (1979).
[32] R. J. Furnstahl, D. R. Phillips, and S. Wesolowski, J. Phys. G **42**, 034028 (2015).
[33] S. K. Bogner, A. Schwenk, R. J. Furnstahl, and A. Nogga, Nucl. Phys. A **763**, 59 (2005).
[34] K. Hebeler, S. K. Bogner, R. J. Furnstahl, A. Nogga, and A. Schwenk, Phys. Rev. C **83**, 031301 (2011).
[35] A. Gezerlis, I. Tews, E. Epelbaum, S. Gandolfi, K. Hebeler, A. Nogga, and A. Schwenk, Phys. Rev. Lett. **111**, 032501 (2013).
[36] T. Krüger, I. Tews, K. Hebeler, and A. Schwenk, Phys. Rev. C **88**, 025802 (2013).
[37] L. Coraggio, J. W. Holt, N. Itaco, R. Machleidt, and F. Sammarruca, Phys. Rev. C **87**, 014322 (2013).
[38] L. Coraggio, J. W. Holt, N. Itaco, R. Machleidt, L. E. Marcucci, and F. Sammarruca, Phys. Rev. C **89**, 044321 (2014).
[39] F. Sammarruca, L. Coraggio, J. W. Holt, N. Itaco, R. Machleidt, and L. E. Marcucci, Phys. Rev. C **91**, 054311 (2015).

[40] L. E. Marcucci, A. Kievsky, S. Rosati, R. Schiavilla, and M. Viviani, Phys. Rev. Lett. **108**, 052502 (2012).
[41] J. Carlson, S.-Y. Chang, V. R. Pandharipande, and K. E. Schmidt, Phys. Rev. Lett. **91**, 050401 (2003).
[42] J. Carlson, Stefano Gandolfi, and Alexandros Gezerlis, Prog. Theor. Exp. Phys. **2012**, 01A209 (2012).
[43] I. Bloch, J. Dalibard, and W. Zwerger, Rev. Mod. Phys. **80**, 885 (2008).
[44] T. Krüger, K. Hebeler, and A. Schwenk, Phys. Lett. B **744**, 18 (2015), and references therein.
[45] D. Alonso and F. Sammarruca, Phys. Rev. C **67**, 054301 (2003).
[46] E. Marji, A. Canul, Q. MacPherson, R. Winzer, Ch. Zeoli, D. R. Entem, and R. Machleidt, Phys. Rev. C **88**, 054002 (2013).
[47] D. R. Entem and R. Machleidt, Phys. Rev. C **68**, 041001 (2003).
[48] R. Machleidt and D. R. Entem, Phys. Rep. **503**, 1 (2011).
[49] J. W. Holt, N. Kaiser, and W. Weise, Phys. Rev. C **81**, 024002 (2010).
[50] K. Hebeler and A. Schwenk, Phys. Rev. C **82**, 014314 (2010).
[51] S. Ishikawa and M. R. Robilotta, Phys. Rev. C **76**, 014006 (2007).
[52] V. Bernard, E. Epelbaum, H. Krebs, and Ulf-G. Meißner, Phys. Rev. C **77**, 064004 (2008).
[53] V. Bernard, E. Epelbaum, H. Krebs, and Ulf-G. Meißner, Phys. Rev. C **84**, 054001 (2011).
[54] J. W. Holt, N. Kaiser, and W. Weise, Phys. Rev. C **79**, 054331 (2009).
[55] N. Kaiser, Eur. Phys. J. A **48**, 148 (2012).
[56] A. Akmal, V. R. Pandharipande, and D. G. Ravenhall, Phys. Rev. C **58**, 1804 (1998).